

“Cellular Network Densification Increases Radio-Frequency Pollution”: True or False?

Luca Chiaraviglio,^(1,2) Sara Turco,^(1,2) Giuseppe Bianchi,^(1,2), Nicola Blefari-Melazzi,^(1,2)

(1) Department of Electronic Engineering,

University of Rome Tor Vergata, Rome, Italy, email {luca.chiaraviglio,giuseppe.bianchi,blefari}@uniroma2.it

(2) Consorzio Nazionale Interuniversitario per le Telecomunicazioni, Italy, email sara.turco@cnit.it

Abstract—A very popular theory circulating among non-scientific communities claims that the massive deployment of Base Stations (BSs) over the territory, a.k.a. cellular network densification, always triggers an uncontrolled and exponential increase of human exposure to Radio Frequency “Pollution” (RFP). To face such concern in a way that can be understood by the layman, in this work we develop a very simple model to compute the RFP, based on a set of worst-case and conservative assumptions. We then provide closed-form expressions to evaluate the RFP variation in a pair of candidate 5G deployments, subject to different densification levels. Results, obtained over a wide set of representative 5G scenarios, dispel the myth: cellular network densification triggers an RFP decrease (up to three orders of magnitude) when the radiated power from the BS is adjusted to ensure a minimum sensitivity at the cell edge. Eventually, we analyze the conditions under which the RFP may increase when the network is densified (e.g., when the radiated power does not scale with the cell size), proving that the amount of RFP is always controlled. Finally, the results obtained by simulation confirm the outcomes of the RFP model.

Index Terms—cellular network, cellular network densification, 5G cellular networks, radio frequency “pollution”, human exposure

I. INTRODUCTION

Unlike past generations cellular systems, the ongoing deployment of 5G networks is surprisingly raising severe debates and strong concerns among the population, to the extent that 5G is sometimes even perceived as a threat. In general, the installation of base stations (BSs) over the territory (called next-generation Node-Bs (gNBs) in 5G) often generates a sentiment of suspect and/or fear, since Radio-Frequency (RF) exposure from BSs is connected to the emergence of severe health effects [2]. Although the causal correlation between RF exposure below the limits defined by laws and long-term effects over humans has not been scientifically (and widely) proven so far by the research community (see e.g., the recent surveys [3], [4]), the continuous fabrication of myths and false claims about health effects due to BS exposure fuels a diffuse negative feeling against this technology [5], leading to sabotages of towers hosting cellular equipment [6], and even 5G installation bans promoted by countries/municipalities [7]–[10].

In this scenario, part the population is firmly convinced that the installation of a massive number of BSs over the territory - a step often known as cellular network densification - results into an uncontrolled and unacceptable increase of human

exposure to Radio Frequency “Pollution” (RFP).¹ Actually, the underlying intuitive (sic!) layman argument is that the RFP directly depends on the amount of deployed antennas: the greater the number of Electro-Magnetic Field (EMF) sources (in terms of BSs), the greater and more dangerous the relevant EMF exposure. And even if any student or practitioner in telecommunications engineering would readily spot the bias in this argument (as the power emitted by BSs is not an *a-priori* fixed parameter), announcements about dramatical increases of RFP due to cellular network densification are frequently spreading across social networks and on newspapers [11].

In this context, two natural questions emerge, namely: How does cellular network densification influence RFP? And is the alleged RFP increase due to BS densification corroborated by scientific evidence? Our goal is to provide an answer to these intriguing questions. Although the scientific community well knows that cellular network densification does not lead in general to an uncontrolled increase of RFP, to the best of our knowledge, there is a huge gap between the research outcomes on one side and their comprehension level by the population on the other one. In more detail, answering to the aforementioned questions in a way that can be understood by the layman is still an underrated and relatively neglected aspect so far. To face this gap, in this work we develop a very simple mathematical model to assess the RFP increase/decrease when comparing two candidate 5G deployments (e.g., a sparse set vs. a dense one). Our model, which can be potentially understood even by the general public (with basic mathematical skills), is based on a set of simplifying (but worst-case) assumptions that allow us to derive closed-form expressions for the RFP, given as input parameters the main wireless features that characterize a 5G deployment, e.g., the adopted frequency, the propagation conditions, the coverage size of the cell, the deployment tessellation and the setting for the maximum radiated power of the cells. By comparing the RFP across pairs of candidate 5G deployments, we are able to assess the impact of cellular network densification and consequently to provide an answer based on scientific evidence to the population concerns.

In order to derive a meaningful set of results, we consider two extreme - yet meaningful - rules to set the radiated power for each gNB, denoted as Minimum Sensitivity-based Power (MSP) and Exposure Limit-based Power (ELP), respectively.

¹The term “pollution” is intentionally left inside quotation marks because it is commonly used by the population rather than by the scientific community, who generally adopts more neutral terms like exposure, radiation, and emission.

With MSP, the radiated power ensures a minimum sensitivity threshold at the gNB edge (and therefore it scales with the BS coverage area). With ELP, the radiated power is set to ensure a stringent EMF limit enforced by law (and therefore it does not scale with the BS coverage area). Our outcomes demonstrate that cellular network densification does not increase the RFP when MSP is adopted. On the other hand, we show that ELP may actually increase the RFP as the network is densified. However, there are conditions under which the RFP is decreased even with this policy, e.g., when the BS operating frequency is increased. In all cases, however, the RFP variation is always controlled. Eventually, we show that the outcomes of our RFP model are confirmed by the numerical values obtained by simulation.

A. Limitations of our work

Clearly, the scope of our work is not to provide an omniscient evaluation of pollution from cellular networks, but rather to focus on a specific feature: the proliferation of BSs of the same type over the territory, i.e., a step normally referred as *horizontal* densification [12]. Other specific technology features, which include 5G functionalities like dynamic beamforming, massive multiple-input multiple-output (MIMO) and/or multiple layers of gNBs covering the same area of territory (a.k.a. *vertical* densification), may introduce a variation in the RFP levels w.r.t. the results presented in this work. To this aim, preliminary results in [13] suggest that densification may be effective in reducing the RFP of beamforming in 5G networks, mainly because the propagation conditions between the serving gNB and the user are improved. However, a deeper evaluation of this aspect is left for future work.

B. Work Organization

The rest of the paper is organized as follows. Sec. II reports the positioning of our work w.r.t. the literature. Sec. III presents the RFP model. Sec. IV details the considered 5G scenarios. Sec. V evaluates the RFP over the different 5G scenarios. Finally, Sec. VI summarizes the paper and points out possible future activities.

II. RELATED WORKS

In terms of related works, we could not find papers similar to ours, i.e., specifically focused on the relation between cellular network densification and RFP. For this reason, in what follows, we position our work w.r.t. the relevant literature appeared in the following related areas: *i*) performance assessment of 5G densification, *ii*) network planning of dense 5G networks, and *iii*) exposure concerns of 5G networks.

A. Performance Assessment of 5G Densification

The works falling inside this category [14]–[21] aim at evaluating the impact of 5G densification on the network performance. To this purpose, Thurfjell *et al.* [14] demonstrate that the user bit rate tends to improve when the network is densified. However, the benefits in terms of capacity may be negatively impacted by the level of interference from the

neighboring cells, as well as changes in the path loss exponents, as pointed out by the same authors. The performance limits of network densification are further analyzed by Nguyen and Kountouris, [15], demonstrating that the user performance increases up to a certain level of densification, after which a saturation or even decay with increasing network density is observed. Moreover, the asymptotic behavior of spectral efficiency is faced by Park *et al.* [18], showing that this metric always grows with increased densification levels. According to Andrews *et al.* [20], the Signal-to-Interference plus Noise Ratio (SINR) initially increases as the 5G network is densified and then decreases after a given level of 5G densification.

Other effects triggered by 5G densification include constraints on the required backhaul network capacity [17], large requirements in terms of backhaul energy consumption [17] and increasing handover rates [19]. Moreover, possible approaches to enhance network capacity are analyzed by Liu *et al.* [16], due to the fact that short-range propagation conditions tend to change in ultra-dense networks w.r.t. legacy ones. Eventually, the importance of introducing interference cancellation mechanisms as network is densified is pointed out by Shafi *et al.* [21]. Finally, densification will be an important feature also in beyond-5G cellular networks, as claimed by Dang *et al.* [22].

Summarizing, the performance gains and the fundamental limits of 5G densification are thoroughly analyzed by the related literature. Despite we recognize the importance of such previous works, none of them investigate the impact of densification on the RFP, which is a major concern for the population and the main goal of this paper.

B. Planning of 5G Dense Cellular Networks

Works [23]–[25] focus on the design of 5G dense cellular networks under costs, coverage and regulatory constraints. The overall problem, often known as 5G network planning, aims at minimizing CAPEX and OPEX costs for the installed gNBs, as well as at properly configuring each installed site in terms of, e.g., radiating elements, antenna configurations, maximum radiated power from each RF element, etc. Clearly, the CAPEX costs tend to notably increase when the inter-site distance is reduced (and consequently the densification level is increased), as shown by Oughton *et al.* [23]. In addition, the planning of dense cellular networks is severely limited in countries ensuring strict EMF limits [24], which prevent the installation of new gNBs over the territory, due to the fact that the overall exposure levels from legacy technologies (e.g., radio/TV repeaters, 2G/3G/4G Base Stations) are already close to the maximum EMF limits. Eventually, the importance of regulatory updates to support the planning of dense 5G networks is stressed by [25].

Although we recognize the importance of the 5G planning problem, only a subset of previous works (e.g., [24], [25]) consider EMF constraints, without however evaluating the impact of different densification levels on the RFP. In contrast to them, our goal is to provide a simple - yet effective - model to compute the RFP level of a cellular network, and to evaluate

the variation on the RFP when the network is densified. Clearly, the RFP contributions from legacy technologies are intentionally not treated in this work, since our goal is to assess the RFP from 5G deployments.

C. Exposure Concerns from 5G Networks

A third group of works [3], [4], [26] is instead tailored to the analysis and assessment of exposure concerns from 5G networks. Simkó and Mattsson [3] review the related literature about health effects from 5G (and pre-5G) exposure, concluding that there is not a consistent relation between health effects and exposure levels, exposure durations or frequency. However, the authors point out that a meaningful safety assessment can not be retrieved from the available studies, and so further researches are needed e.g., to thoroughly assess the (possible) health implications of non-thermal effects triggered by 5G exposure. The impact of 5G on the levels of exposure is also discussed by the Institute of Electrical and Electronics Engineers (IEEE) Committee on Man and Radiation in [4]. In particular, the committee members point out that 5G densification will increase the downlink signal levels, which in turn may reduce the radiated power in the uplink radiation, and hence the exposure from terminals. In addition, the exposure levels will remain lower than the maximum limits ensured by the regulations (based on the guidelines promoted by international organizations such as IEEE [27] and International Commission on Non-Ionizing Radiation Protection (ICNIRP) [28]), even when the network is densified [4]. Finally, Colombi *et al.* [26] perform an exposure assessment in a commercial 5G network, demonstrating that the maximum time-averaged power per beam direction is notably lower than the theoretical maximum. Consequently, the concerns associated with very high exposure levels generated by 5G gNBs are not justified in practice.

In contrast to these works, we do not directly address the relation between EMF exposure and health. Rather, we aim at *quantifying* the RFP when the cellular network is densified. In particular, we demonstrate that there are conditions under which cellular network densification triggers an RFP reduction, which is in turn beneficial in alleviating the exposure concerns.

III. RADIO FREQUENCY “POLLUTION” MODEL

In this section, we describe the main building blocks that characterize our RFP model, and namely: *i*) main assumptions, *ii*) RFP definition, *iii*) radiated power setting, *iv*) cell RFP model, *v*) RFP model at fixed distance, *vi*) RFP upper bound from neighbors, and *vii*) RFP ratio among 5G deployments.

A. Main Assumptions

Our model leverages some standard topological/regularity/propagation assumptions, namely:

- 1) The gNBs are placed on a regular layout, as we consider a dense urban deployment with a uniform distribution of users; consequently, each gNB serves a portion of the total territory under consideration. This assumption is inline with the 5G scenarios defined by relevant standardization bodies (such as 3rd Generation Partnership

Project (3GPP)), which adopt regular deployments and regular cell layouts for urban case-studies [29];²

- 2) All the gNBs of a given deployment are characterized by common features in terms of coverage shape, coverage size, maximum radiated power and adopted frequency; i.e., the same gNB equipment is used across the set. This assumption is motivated by the fact that our goal is to evaluate the proliferation of the same type of gNBs, i.e., the horizontal densification.³
- 3) The propagation conditions are the same among the gNBs in the set; e.g., the reliable coverage distance is sufficiently short to avoid modifications of the propagation model due to changes in the path loss exponent [30].⁴ To this aim, we employ coverage distances in the ranges specified by 3GPP for urban deployments [29].

In addition, another key feature that is assumed in this work is an omnidirectional pattern to characterize the gNB radiation. Clearly, a real 5G gNB generally exhibits a radiation pattern different than a omnidirectional one, because: *i*) sectorization is in general exploited, and *ii*) the extensive adoption of beamforming allows concentrating the transmitted signal strength on specific territory locations. With sectorization, the radiation patterns match the orientation of the sectors. With beamforming, the actual RFP level that is received over the territory generally varies both in time and space, and it is normally estimated through statistical models, which demonstrate that the average RFP at a given pixel is substantially lower than the theoretical maximum value [26], [31]. In our case, assuming an omnidirectional radiation is a worst case scenario, in which: *i*) each pixel of the territory is served by a beam (i.e., the beams are simultaneously activated in all the directions), *ii*) each pixel is not affected by sectorization (i.e., for a given pixel to gNB distance, the user equipment (UE) received power is constant across the entire geographic extent of the sector, even for pixels along the sector edge).

In more detail, the omni-directional assumption leads to an over-estimation of the received RFP, which substantiates our results. Let us provide more explanations about this aspect, by first assuming that not all beams are activated all together at the same time. In this case, a subset of beams is activated to cover only the zones where the users are currently located. Interestingly, our model correctly estimates the RFP for the zones exposed to the active beams. On the other hand, the zones that are not served by the beams are subject to a negligible amount of pollution. Therefore, in this scenario, our conclusions are valid for the pollution received by the served users. In other cases, however, the RFP may be higher than the one estimated in this work. Such additional scenarios include: *i*) multiple beams simultaneously serving multiple users over the same portion of territory and/or *ii*) each user

²Clearly, other scenarios (including e.g., a mixture of urban/rural areas and/or non-uniform distribution of users) may require a different modeling for the positions of gNBs and/or users, based e.g., on stochastic geometry tools. We leave the investigation of such aspects as future work.

³The investigation of the impact of heterogeneous 5G networks (i.e., composed of multiple layers of gNBs simultaneously providing coverage over the same area) is left for future work.

⁴The integration of more complex propagation models, e.g., based on a dual slope, is left for future work.

simultaneously served by more than one beam. Despite we recognize the importance of scenarios *i-ii*), we point out that in many countries the currently adopted option to deploy 5G gNBs is to use static and non overlapping beams (see e.g., the recent work of [32]). Moreover, power lock mechanisms are under study to turn off the beam(s) if the overall exposure is excessive [33]. Eventually, preliminary results in [13] demonstrate that densification is beneficial in reducing the exposure in networks applying dynamic beamforming, mainly because the propagation conditions between the serving gNB and the user are improved, thus yielding to a decrease of the power radiated by the beam.

B. RFP Definition

In this work, the RFP is defined as the amount of power that is received over a given pixel p from the serving gNB s and from each gNB i in the neighborhood $\mathcal{T}^{\text{NEIGH}}$. Actually, other alternative metrics that can be exploited to characterize RFP include EMF strength, Power Density (PD) and/or Specific Absorption Rate (SAR). We refer the interested reader to [34] for an overview about the main RFP metrics. Henceforth, we consider the received power as the reference metric, due to the following reasons: *i*) we exploit well-known propagation models derived from telecommunications research (see e.g., [30]) to compute the RFP levels over the territory, *ii*) we consider different rules, including a minimum sensitivity threshold at the cell edge, to set the gNB radiated power.

Let us assume a standard propagation model [30], in which the received RFP depends on the power radiated by the gNBs, scaled by the propagation parameters. More formally, the total RFP $P_{(p)}^R$ over pixel p is denoted as:

$$P_{(p)}^R = \underbrace{\frac{P^E}{d_{(p,s)}^\gamma \cdot f^\eta \cdot c}}_{\text{RFP from serving gNB}} + \sum_{i \in \mathcal{T}^{\text{NEIGH}}} \underbrace{\frac{P^E}{d_{(p,i)}^\gamma \cdot f^\eta \cdot c}}_{\text{RFP from neighboring gNBs}}, \quad (1)$$

where P^E is the gNB emitted power, $d_{(p,s)}$ [m] is the distance between the serving gNB s and the current pixel p , γ is the propagation exponent for the distance, f [GHz] is the operating frequency, η is the frequency exponent, c is a constant integrating other effects (e.g., the fixed term in the Friis' free space equation [35]), and $d_{(p,i)}$ [m] is the distance between neighboring gNB i and the current pixel p .

By observing in more detail Eq. (1), we can note that the RFP significantly differs w.r.t. other metrics commonly adopted for energy and/or performance evaluations (e.g., area power efficiency, area spectral efficiency and peak power), which either include the contribution of neighbors as interference or they only consider the power of the serving gNB. In our work, the RFP is the summation of power from all the gNBs that contribute to the exposure (i.e., both serving and interfering ones).

Clearly, a natural question is: How do we select the serving gNB s and the neighboring gNBs i for a given pixel p appearing in Eq. (1)? To this aim, we assume a circular coverage area of radius d_{MAX} , which corresponds to the maximum coverage distance. In addition, we introduce a minimum distance d_{MIN}

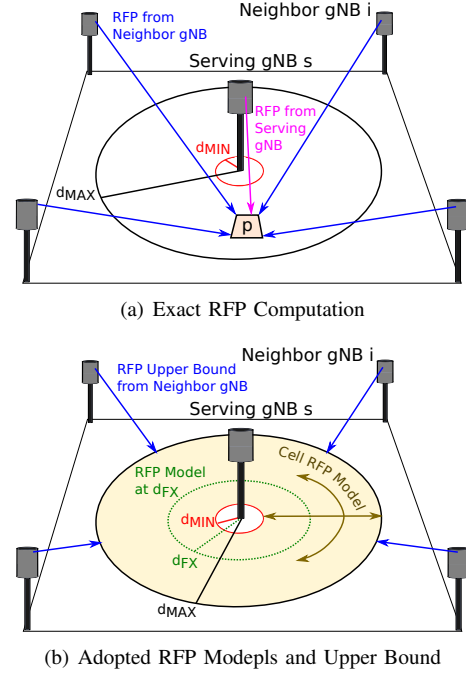


Fig. 1. Exact RFP computation over a single pixel p (a) vs. adopted RFP models and upper bound (b).

to model the presence of an exclusion zone in proximity to the gNB. In line with the international recommendations [36] and the exposure assessment standards [37], the exclusion zone access is forbidden to the general public, and therefore this zone is not considered in the RFP computation. Consequently, gNB s serves pixel p if $d_{\text{MIN}} \leq d_{(p,s)} \leq d_{\text{MAX}}$. Focusing then on the neighboring gNBs, in this work we assume that the closest $|\mathcal{T}^{\text{NEIGH}}| = N^I$ gNBs w.r.t. s contribute to the RFP. Moreover, we consider different values of N^I to evaluate its impact on the RFP.

Since our goal is to provide a simple model, we leverage a further worst-case approximation which permits to dramatically simplify computations, and neglects the specific distances $d_{(p,i)}$ from the neighbors appearing in Eq. (1). Such key assumption consists in bounding the “true” distance $d_{(p,i)}$ from neighbor i with a *constant* (and shorter) distance between each neighbor and the pixel in the target coverage area closer to it, i.e., at the cell edge. This worst-case assumption, which will formally presented as an Upper Bound (UB) in Sec. III-F, yields a constant and same RFP from neighbors for every considered pixel in the coverage area, and allows us to obtain simple closed-form form RFP expressions that only depend on N^I .

To give more insight, Fig. 1(a) shows a graphical example of the RFP terms appearing in Eq. (1) in a simple toy-case scenario composed of five gNBs. The considered pixel p falls inside the serving area of gNB s . Consequently, the RFP is computed from the serving gNB s and the neighboring $N^I = 4$ gNBs. Fig. 1(b) then provides a graphical overview on how the RFP computation of Eq. (1) is simplified in our models. In particular, we introduce: *i*) a model to compute the RFP over the whole area of the serving gNB, a.k.a. cell RFP model, *ii*) a model to compute the RFP at a given distance d_{FX} from the

servicing gNB, a.k.a. RFP model at fixed distance, and *iii*) a UB to estimate the RFP from neighbors. In parallel, we also build a simulator to compare the outcomes of our models w.r.t. the exact RFP computation of Eq. (1).

C. Radiated Power Setting

Before unveiling the details of our RFP models, let us now focus on the radiated power P^E appearing in the RFP definition of Eq. (1). Clearly, the value assigned to P^E plays a key role in determining the level of RF ‘‘Pollution’’. Intuitively, the higher is the radiated power, the higher is also the RFP over the territory. Therefore, a careful setting of P^E is crucial for a meaningful RFP evaluation. We remind that, in this work, we consider two distinct rules to set P^E , namely: *i*) a MSP setting and *ii*) an ELP one. In the following, we formally describe such policies.

1) *Minimum Sensitivity-based Power Setting (MSP)*: The goal of MSP is to tune P^E in order to ensure a minimum sensitivity threshold P_{TH}^R at the cell edge d_{MAX} . We recall that the minimum sensitivity is reported in relevant 5G 3GPP standards [38]. In particular, P_{TH}^R is defined as the minimum mean power applied to each one of the UE antenna ports in order to meet the throughput requirements. By imposing a minimum sensitivity constraint, we ensure that the throughput is larger than 95% of the maximum throughput of the reference measurement channels for the users in the worst propagation conditions (i.e., the ones located at the cell edge).

More formally, we assume the same propagation model of Eq. (1) to define the radiated power P^E :

$$P^E = P_{\text{TH}}^R \cdot d_{\text{MAX}}^\gamma \cdot f^\eta \cdot c. \quad (2)$$

By replacing Eq. (2) in Eq. (1) (and without considering the contributions from neighbors), it is trivial to verify that $P_{(p)}^R = P_{\text{TH}}^R$ for the pixel(s) at d_{MAX} .

By observing in more detail Eq. (2), we can note that the MSP setting increases the radiated power when the cell size is widened (i.e., d_{MAX} increase), when the propagation conditions are worsened (i.e., γ increase) and/or when the adopted gNB frequency f is increased.

2) *Exposure Limit-based Power Setting (ELP)*: We then consider a second alternative policy for setting P^E , which matches the actual power settings in countries imposing strict EMF limits [12]. When strict EMF limits are imposed, in fact, the power radiated by gNBs is strongly influenced by the exposure limits for the general public, which have to be ensured in each pixel of the territory (outside the gNB exclusion zone) [24]. Such limits are in general, much more stringent than the international ones [28], and typically impose strong limitations on the setting of the power radiated by each gNB [24]. In this scenario, when a strict exposure limit has to be enforced, the tightest constraint in network deployment is not performance (like in the MSP case), but rather the strict EMF exposure limit. To this aim, we refer the interested reader to [39] for more details about the impact of strict exposure limits on the performance of mobile networks (including 5G).

More formally, we adopt the procedure defined by International Telecommunication Union (ITU)-T REC K.70 [40] to

verify the adherence w.r.t. the EMF limits, by performing the following steps: *i*) we compute the total PD that is received by a given pixel from a set of gNBs, and *ii*) we verify that the total received PD is lower than the maximum PD limit S_{MAX} for all the pixels outside the gNB exclusion zone. Focusing on *i*), we apply the point-source model [40] because the PD computed with this approach is always a UB of the actual level of exposure, and hence a worst-case scenario. More formally, each gNB is characterized by a given transmission gain G_{TX} and a given transmission loss L_{TX} . The received PD $S_{(p,s)}$ by pixel p from gNB s is then expressed as in [40]:

$$S_{(p,s)} = \underbrace{\frac{P^E \cdot G_{\text{TX}}}{4\pi \cdot L_{\text{TX}} \cdot d_{(p,s)}^2}}_{\text{Point-source model}}. \quad (3)$$

In order to satisfy the EMF limits, the total received PD has to be lower than the maximum one:

$$\underbrace{\frac{P^E \cdot G_{\text{TX}}}{4\pi \cdot L_{\text{TX}} \cdot d_{(p,s)}^2}}_{\text{PD from serving gNB } S_{(p,s)}} + \sum_{i \in \mathcal{I}^{\text{NEIGH}}} \underbrace{\frac{P^E \cdot G_{\text{TX}}}{4\pi \cdot L_{\text{TX}} \cdot d_{(p,i)}^2}}_{\text{PD from neigh. gNB } S_{(p,i)}} \leq \underbrace{S_{\text{MAX}}}_{\text{PD Limit}} \quad (4)$$

By observing in more detail Eq. (4), we can note that the maximum PD is likely experienced in proximity to s , where the PD contribution from the serving gNB s dominates over the one from the neighbors, because $d_{(p,s)} \ll d_{(p,i)}$. This finding is also corroborated by EMF measurements performed over real cellular networks under operation [41]. Therefore, a sufficient condition to satisfy Eq. (4) is to verify that the PD from the serving gNB s , evaluated at distance d_{MIN} , is lower than the PD limit S_{MAX} :

$$\underbrace{\frac{P^E \cdot G_{\text{TX}}}{4\pi \cdot L_{\text{TX}} \cdot d_{\text{MIN}}^2}}_{\text{PD at minimum distance}} \leq S_{\text{MAX}}. \quad (5)$$

Consequently, the previous inequality is satisfied when P^E is set equal to:

$$P^E = 4\pi \cdot d_{\text{MIN}}^2 \cdot S_{\text{MAX}} \cdot \frac{L_{\text{TX}}}{G_{\text{TX}}}. \quad (6)$$

By setting P^E in accordance with Eq. (6), the radiated power does not depend neither on the maximum coverage distance d_{MAX} , the frequency f or the propagation exponent γ , but solely on the exposure limit S_{MAX} , the transmission gain G_{TX} , the transmission loss L_{TX} and the minimum distance d_{MIN} . Clearly, when stringent EMF limits are assumed for S_{MAX} , this policy dominates over the MSP setting, because the operator always aims at saturating the radiated power to the maximum allowed one.

D. Cell RFP Model

In the following, we define a model to capture the RFP across the entire cell with a closed-form expression. Our intuition is, in fact, to derive in a compact way the RFP from the serving gNB s of Eq. (1) for all the pixels p belonging to its coverage area. By assuming an infinitesimal pixel size, we

express the average RFP over the entire area \mathcal{A} served by the gNB as:

$$P_{\text{CELL}}^R = \frac{1}{\pi(d_{\text{MAX}}^2 - d_{\text{MIN}}^2)} \int \int_{\mathcal{A}} \frac{P^E}{(\sqrt{x^2 + y^2})^\gamma \cdot f^\eta \cdot c} dx dy, \quad (7)$$

where $\frac{1}{\pi(d_{\text{MAX}}^2 - d_{\text{MIN}}^2)}$ is the inverse of the served area and $\sqrt{x^2 + y^2}$ is the distance from the gNB center to a generic point (x, y) .

In order to solve Eq. (2), we adopt a reference system based on polar coordinates, where: $x = r \cos \theta$, $y = r \sin \theta$, $dx dy = r dr d\theta$. Therefore, Eq. (7) is rewritten as:

$$P_{\text{CELL}}^R = \frac{1}{\pi(d_{\text{MAX}}^2 - d_{\text{MIN}}^2)} \int_0^{2\pi} \int_{d_{\text{MIN}}}^{d_{\text{MAX}}} \frac{P^E}{r^{(\gamma-1)} \cdot f^\eta \cdot c} dr d\theta. \quad (8)$$

We then consider the solution of Eq. (8) for $\gamma \in (2, 4]$, i.e., a typical range for characterizing Line-of-Sight (LOS)/Non-Line of Sight (NLOS) conditions w.r.t. urban macro/micro cells [30],⁵ thus obtaining the following closed-form RFP expression:

$$P_{\text{CELL}}^R = \frac{2P^E}{(d_{\text{MAX}}^2 - d_{\text{MIN}}^2) \cdot f^\eta \cdot c \cdot (\gamma - 2)} \cdot \left[\frac{1}{d_{\text{MIN}}^{(\gamma-2)}} - \frac{1}{d_{\text{MAX}}^{(\gamma-2)}} \right] \quad (9)$$

In this way, we have derived a simple model to compute the cell RFP over the whole area served by a given gNB. By observing in more detail Eq. (9), we can note that P_{CELL}^R is strongly influenced by the propagation exponent γ (as expected), which results into different scaling factors for the radiated power P^E . Other parameters that affect P_{CELL}^R include the adopted frequency f , the constant term c , as well as the distances d_{MIN} and d_{MAX} .

E. RFP Model at Fixed Distance

We then provide a second model to evaluate the RFP from the serving gNB. In particular, let us now consider a generic pixel at a fixed distance d_{FX} from the serving gNB. The RFP P_{FX}^R at distance d_{FX} from the serving cell is then formally expressed as:

$$P_{\text{FX}}^R = \frac{P^E}{d_{\text{FX}}^\gamma \cdot f^\eta \cdot c}. \quad (10)$$

By varying d_{FX} in the previous equation, we compute the RFP over different evaluation points from the serving gNB. For example, we can compute the RFP in close proximity to the minimum distance d_{MIN} , whose pixels are subject to the highest RFP levels.

F. RFP Upper Bound from Neighboring Cells

In the following, we provide a UB to estimate the RFP from N^I neighboring gNB. Let us denote with d_{SITE} the inter-site distance between a pair of neighboring gNBs. By assuming that the sites hosting gNBs are positioned with a

⁵The border value $\gamma = 2$ leads to $P_{\text{CELL}}^R = \frac{2P^E}{(d_{\text{MAX}}^2 - d_{\text{MIN}}^2) \cdot f^\eta \cdot c} \cdot [\ln(d_{\text{MAX}}) - \ln(d_{\text{MIN}})]$, which is however not further discussed in this work as $\gamma > 2$ under commonly observed propagation conditions [30].

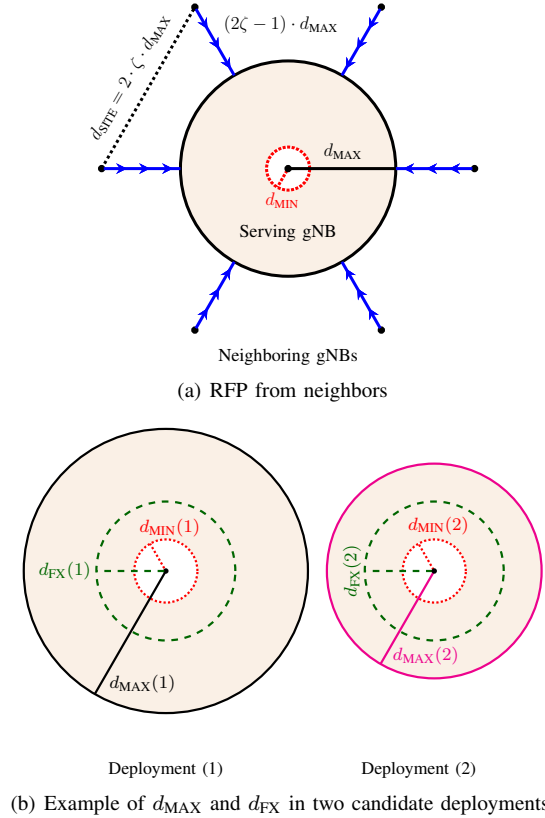


Fig. 2. (Left) Graphical sketch of the distances appearing in the RFP computation from the neighbors of Eq. (12). The RFP from neighboring gNBs is evaluated at $(2\zeta - 1) \cdot d_{\text{MAX}}$. (Right) d_{MAX} , d_{MIN} and d_{FX} in two candidate deployments. Clearly, $d_{\text{MAX}}(2) < d_{\text{MAX}}(1)$, while $d_{\text{FX}}(2) = d_{\text{FX}}(1)$ and $d_{\text{MIN}}(2) = d_{\text{MIN}}(1)$. Figures best viewed in colors.

regular deployment, the relationship between d_{SITE} and d_{MAX} is expressed as:

$$d_{\text{SITE}} = 2\zeta \cdot d_{\text{MAX}}, \quad (11)$$

where $\zeta \in (0, 1)$ is a geometric parameter that is introduced to avoid coverage holes over the whole territory under consideration. Our idea is then to assume a fixed contribution from each neighbor, which is computed at the edge of the serving gNB. More formally, the RFP from neighbors is expressed as:

$$P_{\text{NEIGH}}^R = N^I \frac{P^E}{d_{\text{MAX}}^\gamma \cdot (2\zeta - 1)^\gamma \cdot f^\eta \cdot c}. \quad (12)$$

To give more insight, Fig. 2(a) reports a graphical example of the d_{MAX} and ζ terms appearing on the right-hand side of Eq. (12), by assuming a hexagonal deployment of gNB sites and $N^I = 6$. Clearly, the value of N^I depends on the chosen geometry for placing the gNBs, which in this case is a hexagonal grid. Therefore, Eq. (12) includes the contributions of first-level neighbors. The contributions of i -th neighbors (where $i \geq 2$) is intentionally omitted, due to the following reasons: *i*) the received power from neighbors is scaled by a factor proportional to $i^{\gamma-1}$ (details are omitted due to the lack of space), thus making the contributions of neighbors mostly irrelevant starting from the second level onwards, and *ii*) the vertical orientation of each cell employs electrical

and/or mechanical tilting to concentrate the radiation over the coverage area and avoid unwanted interference towards the neighboring gNBs.

By observing the figure, it is trivial to verify that Eq. (12) represents a UB of the RFP for each neighbor $i \in \mathcal{I}^{\text{NEIGH}}$ and for each pixel p falling inside the coverage area of the serving gNB, because $(2\zeta - 1) \cdot d_{\text{MAX}} \leq d_{(p,i)}$. In addition, although this UB may appear rather conservative at a first glance, we will show that the impact of neighbors on the total RFP is always limited.

G. RFP Ratio Among 5G Deployments

In the final part of this section, we put together the previous models to evaluate the RFP increase/decrease when comparing a pair of candidate 5G deployments. Let us start by defining the total cell RFP (including the UB from neighbors) as:

$$P_{\text{TOT-CELL}}^R = P_{\text{CELL}}^R + P_{\text{NEIGH}}^R. \quad (13)$$

In a similar way, the total RFP at fixed distance is equal to:

$$P_{\text{TOT-FX}}^R = P_{\text{FX}}^R + P_{\text{NEIGH}}^R. \quad (14)$$

Let us now consider two distinct 5G deployments, which are denoted by indexes (1) and (2), respectively. Each 5G deployment is characterized by specific settings in terms of densification level (and hence maximum coverage distance d_{MAX}), as well as the other parameters including e.g., the adopted frequency f , the propagation exponent γ , etc. We then define the cell RFP ratio among the two deployments as:

$$\delta(P_{\text{TOT-CELL}}^R) = \frac{P_{\text{TOT-CELL}}^R(1)}{P_{\text{TOT-CELL}}^R(2)}. \quad (15)$$

In particular, when $\delta(P_{\text{TOT-CELL}}^R) > 1$, deployment (1) pollutes more than deployment (2). The opposite holds when $\delta(P_{\text{TOT-CELL}}^R) < 1$. On the other hand, when $\delta(P_{\text{TOT-CELL}}^R) = 1$, no change in the total cell RFP is observed among the two deployments. Since an UB is used to express the RFP from neighbors, $\delta(P_{\text{TOT-CELL}}^R)$ may naturally differ w.r.t. the “real” RFP ratio (i.e., the one computed with the actual distance from neighbors, as in Eq. (1)). To face this issue, we compare in this work the $\delta(P_{\text{TOT-CELL}}^R)$ values computed from the model against the “real” RFP ratio computed by simulation. The theoretical proof of the approximation introduced by Eq. (15) is left for future work. In general, the outcomes of our model may be useful to distinguish between the cases $\delta(P_{\text{TOT-CELL}}^R) < 1$ and $\delta(P_{\text{TOT-CELL}}^R) > 1$, while the results from simulation allows precisely quantifying the RFP variation.

In a similar way, let us introduce the RFP ratio at fixed distance as:

$$\delta(P_{\text{TOT-FX}}^R) = \frac{P_{\text{TOT-FX}}^R(1)}{P_{\text{TOT-FX}}^R(2)}. \quad (16)$$

By varying the parameters assigned to each deployment option, we are able to evaluate their effect on the RFP ratios. For example, the impact of increasing the densification level is evaluated by imposing $d_{\text{MAX}}(2) < d_{\text{MAX}}(1)$. To this aim, a graphical sketch of two candidate deployments, subject to different densification levels, is shown in Fig. 2(b). In this example, deployment (2) is denser than deployment (1), since

TABLE I
RFP PARAMETERS SETTING OVER THE DIFFERENT 5G SCENARIOS.

Set	Param.	S1	S2	S3	S4	S5
Distance	d_{MIN}	5 [m]-15 [m]				
	$d_{\text{MAX}}(1)$	500 [m]				
	$d_{\text{MAX}}(2)$	250 [m]	100 [m]	250 [m]	500 [m]	50 [m]
	$\delta(d_{\text{MAX}})$	2	5	2	1	10
	$\gamma(2)$	3	2.1	3	3	2.1
Frequency	$f(1)$	0.7 [GHz]				
	$f(2)$	0.7 [GHz]	3.7 [GHz]			
	$\delta(f)$	1	0.19			
	η	2				
Baseline	$c(1)$	32.4 [dB]				
	$c(2)$	32.4 [dB]				
	$\delta(c)$	1				
Height	ζ	$\sqrt{3}/2$ (Hexagonal placement of gNB sites)				
	N^I	{0, 6}				
MSP	$P_{\text{TH}}^R(1)$	-90 [dBm]				
	$P_{\text{TH}}^R(2)$	-90 [dBm]		-87 [dBm]		
	$\delta(P_{\text{TH}}^R)$	1		0.5		
ELP	S_{MAX}	0.1 [W/m ²]				
	G_{TX}	15 [dB]				
	L_{TX}	2.32 [dB]				

$d_{\text{MAX}}(2) < d_{\text{MAX}}(1)$. However, $d_{\text{FX}}(2) = d_{\text{FX}}(1)$, i.e., the same observation point is assumed for the RFP at fixed distance. In addition, $d_{\text{MIN}}(2) = d_{\text{MIN}}(1)$, i.e., the same exclusion zone is applied when computing the cell RFP. In the following, we shed light on the adopted 5G scenarios.

IV. DESCRIPTION OF 5G SCENARIOS

Finding meaningful sets of input parameters to compare pairs of candidate 5G deployments is a fundamental step for the RFP evaluation. Therefore, rather than considering a single scenario, which would narrow the scope of the presented outcomes, in this work we evaluate five representative 5G scenarios (denoted with S1-S5), detailed in Tab. I. In this way, we assess the impact of different densification levels (e.g., light, medium and strong) and other relevant parameters that are closely connected to densification, such as the operating frequency f and the propagation exponent γ . We then group the input parameters in Tab. I according to the following scopes: *i*) distance, *ii*) frequency, *iii*) baseline path loss, *iv*) neighbors, *v*) MSP setting, *vi*) ELP setting.

Let us first describe the main features of each parameter group. Focusing on the distance-related parameters, the d_{MAX} values in the table are set as follows: *i*) $d_{\text{MAX}} = 250$ [m] and lower values to represent the urban macro and dense urban deployments of 3GPP [29], respectively; *ii*) $d_{\text{MAX}} = 500$ [m] to reflect sparser deployments (while still keeping d_{MAX} lower than the distance triggering a change in the propagation exponent [30]). Moreover, we introduce the parameter $\delta(d_{\text{MAX}})$ to denote the relative ratio between $d_{\text{MAX}}(1)$ and $d_{\text{MAX}}(2)$. The values of d_{MIN} are set according to typical sizes of gNB exclusion zones (see e.g., [26] with theoretical maximum power). The setting of d_{MIN} is also justified by assuming that each gNB is hosted on the roof of a buildings and/or on top of a radio tower, and therefore the minimum distance between the UE and the gNB is not negligible.⁶ Eventually, the values

⁶In this work, we always consider roof-mounted gNBs, for which the size of exclusion zone is not negligible. The evaluation of other types of gNBs without exclusion zones (e.g., indoor and/or femto gNBs) is left for future work.

of the propagation exponent γ are set by assuming typical LOS/NLOS conditions. In particular, the range $\gamma = (2, 4]$ is adopted for the channel models of 3GPP in urban areas, i.e., 5G Urban Macro LOS/NLOS and 5G Urban Micro - Street Canyon [42].

We then move our attention to the frequency-related parameters. We adopt the 5G Italian frequencies in the sub-6 [GHz] spectrum, which is the most promising option for offering coverage and a mixture of coverage and capacity.⁷ Consequently, we set $f(1) = 0.7$ [GHz] and $f(2) = \{0.7, 3.7\}$ [GHz]. Moreover, we introduce the frequency ratio $\delta(f) = f(1)/f(2)$. Eventually, the η exponent is set in accordance to [30].

Focusing then on the parameters related to baseline path loss, we adopt $c = 32.4$ [dB], in accordance with the Free Space Path Loss (FSPL) model reported by [30]. We remind that this term is derived from the constant part of the Friis' free space equation [35]. Moreover, we introduce the ratio $\delta(c) = c(1)/c(2)$, which is equal to one in our scenarios.

We then analyze the parameters related to the RFP from neighbors. We assume a hexagonal deployment of gNBs sites, thus resulting in $\zeta = \sqrt{3}/2$. In addition, we consider two distinct settings for the number of neighbors N^I when computing the RFP. More in depth, when $N^I = 0$, the RFP is solely due to the serving cell, while no contribution from the neighbors is assumed (thus representing an ideal case). On the other hand, when $N^I = 6$, the RFP includes the contributions from the six closest neighbors w.r.t. the serving gNB.

We then detail the parameters to set the radiated power P^E . When an MSP approach is assumed, we consider values of sensitivity threshold P_{TH}^R slightly higher than the minimum operating ones (defined in [38] for the different 5G frequencies, bands and sub-carrier spacing). In addition, we consider cases in which $P_{\text{TH}}^R(2) > P_{\text{TH}}^R(1)$, i.e., deployment (2) enforces a better sensitivity, and hence a (potential) better service. More formally, the setting $P_{\text{TH}}^R = -90$ [dBm] allows guaranteeing the maximum throughput when up to 20 [MHz] of bandwidth (with 15 [kHz] of subcarrier spacing) is used in the 700 [MHz] frequency, and when up to 30 [Mhz] of bandwidth (with 15 [kHz] of subcarrier spacing) is used in the 3700 [MHz] frequency [38]. In addition, the setting $P_{\text{TH}}^R = -87$ [dBm] allows achieving the maximum throughput up to 70 [MHz] of bandwidth (with 60 [kHz] of subcarrier spacing) [38]. Eventually, we introduce the ratio $\delta(P_{\text{TH}}^R) = P_{\text{TH}}^R(1)/P_{\text{TH}}^R(2)$, whose values are also reported in the table. On the other hand, when the radiated power is set according to ELP, we assume the Italian PD limit for residential areas, i.e., $S_{\text{MAX}} = 0.1$ [W/m²], which we remind is much more stringent than the ones defined in international guidelines, such as the ICNIRP 2020 limits [28]. Moreover, the values of G_{TX} and L_{TX} are set in accordance to [40].

In the following step, we provide a comparative description among the two candidate deployments in S1-S5:

⁷The auction for 5G in Italy included also frequencies above 6 [GHz] (generally called "mm-Waves"), which are however not treated in this work because the installation of gNBs operating on sub-6 [GHz] frequencies is prioritized w.r.t. equipment working on mm-Waves, due e.g., to 5G coverage constraints imposed by the national government. Therefore, it is expected that gNBs operating on mm-Waves will be not immediately and widely deployed. The evaluation of densification on mm-Waves is then left as a future work.

- S1) Light densification scenario. The only parameter (slightly) changing across deployment (1) and deployment (2) is d_{MAX} (and consequently $\delta(d_{\text{MAX}})$). In S1, deployment (2) is slightly denser than deployment (1), while all the other parameters do not vary across the two deployments;
- S2) Moderate densification scenario, which is subject to a radical variation of d_{MAX} and γ across the two deployments. In S2, the operator adopts a denser deployment in (2) compared to (1). This choice is coupled with a different site deployment strategy and/or site configuration setting, which allows a better coverage over the territory. Consequently, $\gamma(2) < \gamma(1)$;
- S3) Light densification with frequency change. In S3, both d_{MAX} and f are varied in the two deployments. Specifically, while the 0.7 [GHz] frequency in (1) is primarily used to provide coverage, the 3.7 [GHz] frequency of deployment (2) allows achieving a good mixture of coverage and capacity. Moreover, we consider a slight reduction of $d_{\text{MAX}}(2)$ compared to $d_{\text{MAX}}(1)$;
- S4) No densification with frequency change. In S4, d_{MAX} is not varied, while f is increased when passing from deployment (1) to deployment (2). When an MSP setting is assumed, this scenario also imposes $P_{\text{TH}}^R(2) > P_{\text{TH}}^R(1)$. With these settings, the operator is able to support a 5G service demanding a higher amount of capacity in deployment (2) compared to (1);
- S5) Strong densification with frequency change. In S5 we impose $d_{\text{MAX}}(2) \ll d_{\text{MAX}}(1)$, $f(2) > f(1)$, and $\gamma(2) < \gamma(1)$. As a consequence, the impact of passing from a sparse set of 5G gNBs to a very dense deployment is evaluated. Clearly, this choice has an impact on the propagation conditions, as users in deployment (2) tend to be in LOS conditions w.r.t. the serving 5G gNB, thus resulting in $\gamma(2) < \gamma(1)$. Moreover, when P^E is set in accordance with MSP, this scenario imposes an increase of the minimum sensitivity P_{TH}^R in deployment (2) compared to (1). Similarly to S4, in S5 the operator provides a larger capacity to the users.

V. RFP EVALUATION

We initially focus on the closed-form expressions for the RFP to scientifically analyze the impact of densification, by considering the same size d_{MIN} of the exclusion zone across the candidate deployments. We then move our attention to the numerical evaluation of the RFP in order to give more insights about the impact of the input parameters on the obtained RFP values. In the following step, we investigate the impact of varying d_{MIN} across the deployments. Eventually, we shed light on the impact of alternative policies (based on the spectrum allocation) to set the radiated power. Finally, we evaluate the RFP when the number of neighbors is increased.

A. Closed-Form RFP Evaluation

As a first step, we retrieve the closed-form expressions for the RFP by assuming $N^I = 0$ and the MSP setting. We remind that, in this way, each gNB solely pollutes its own

TABLE II
CLOSED-FORM EXPRESSIONS FOR RFP RATIO AT FIXED DISTANCE $\delta(P_{\text{TOT-FX}}^R)$ AND CELL RFP RATIO $\delta(P_{\text{TOT-CELL}}^R)$ IN THE DIFFERENT SCENARIOS
WHEN $N^I = 0$ (MSP CASE). TABLE BEST VIEWED IN COLORS.

Scenario	at Fixed Distance $\delta(P_{\text{TOT-FX}}^R)$		RFP Ratio	
	Formula	RFP Increase?	Cell $\delta(P_{\text{TOT-CELL}}^R)$	RFP Increase?
			Formula	
S1	$\delta(d_{\text{MAX}})^3$	No	$\delta(A)^{-1} \cdot \delta(d_{\text{MAX}})^2 \cdot \left[\frac{d_{\text{MAX}}(1) - d_{\text{MIN}}}{d_{\text{MAX}}(2) - d_{\text{MIN}}} \right]$	Num. Eval.
S2	$\frac{\delta(d_{\text{MAX}})^{\gamma(2)}}{\beta(1)^{\gamma(1) - \gamma(2)}}$	No	$\delta(A)^{-1} \cdot \frac{d_{\text{MAX}}(1)^{\gamma(1)}}{d_{\text{MAX}}(2)^{\gamma(2)}} \cdot \frac{\gamma(2) - 2}{\gamma(1) - 2} \cdot \left[\frac{d_{\text{MIN}}^{(2-\gamma(1))} - d_{\text{MAX}}(1)^{(2-\gamma(1))}}{d_{\text{MIN}}^{(2-\gamma(2))} - d_{\text{MAX}}(2)^{(2-\gamma(2))}} \right]$	Num. Eval.
S3	$\delta(d_{\text{MAX}})^3$	No	$\delta(A)^{-1} \cdot \delta(d_{\text{MAX}})^2 \cdot \left[\frac{d_{\text{MAX}}(1) - d_{\text{MIN}}}{d_{\text{MAX}}(2) - d_{\text{MIN}}} \right]$	Num. Eval.
S4	$\delta(P_{\text{TH}}^R)$	Yes	$\delta(P_{\text{TH}}^R)$	Yes
S5	$\frac{\delta(d_{\text{MAX}})^{\gamma(2)} \cdot \delta(P_{\text{TH}}^R)}{\beta(1)^{\gamma(1) - \gamma(2)}}$	Num. Eval.	$\delta(P_{\text{TH}}^R) \cdot \delta(A)^{-1} \cdot \frac{d_{\text{MAX}}(1)^{\gamma(1)}}{d_{\text{MAX}}(2)^{\gamma(2)}} \cdot \frac{\gamma(2) - 2}{\gamma(1) - 2} \cdot \left[\frac{d_{\text{MIN}}^{(2-\gamma(1))} - d_{\text{MAX}}(1)^{(2-\gamma(1))}}{d_{\text{MIN}}^{(2-\gamma(2))} - d_{\text{MAX}}(2)^{(2-\gamma(2))}} \right]$	Num. Eval.

coverage area, i.e., no RFP from neighbors is assumed. In addition, the emitted power is set in order to guarantee the minimum sensitivity thresholds $P_{\text{TH}}^R(1)$ and $P_{\text{TH}}^R(2)$. Let us then introduce the ratio among the coverage areas of a single gNB in the two deployments as:

$$\delta(A) = \frac{\pi(d_{\text{MAX}}(1))^2 - d_{\text{MIN}}^2}{\pi(d_{\text{MAX}}(2))^2 - d_{\text{MIN}}^2}. \quad (17)$$

In addition, let us introduce the β parameter, which is defined as the ratio between the observation point at fixed distance and the maximum coverage distance. More formally, we have $\beta(1) = \frac{d_{\text{FX}}(1)}{d_{\text{MAX}}(1)}$ for deployment (1). Unless otherwise specified, we set: $d_{\text{MIN}} = 15$ [m] for both the deployments (i.e., the same exclusion zone is assumed), $d_{\text{FX}}(1) = d_{\text{MIN}} + 1$ [m], $d_{\text{FX}}(2) = d_{\text{FX}}(1)$, i.e., the RFP at fixed distance is evaluated in close proximity to d_{MIN} .

Tab. II reports the RFP ratio at fixed distance $\delta(P_{\text{TOT-FX}}^R)$ and the cell RFP ratio $\delta(P_{\text{TOT-CELL}}^R)$ over the different scenarios. The color of each cell in the table is set according to the following rule: *i*) green if the expression leads to an RFP decrease, *ii*) red if the expression is lower than one, and hence an RFP increase is experienced, *iii*) white if the RFP expression includes terms that are respectively lower and higher than one, thus requiring a numerical evaluation.

By analyzing the colors of the table, we can note that the RFP at fixed distance is decreased in S1-S3, as the mathematical expressions for $\delta(P_{\text{TOT-FX}}^R)$ include terms that are all greater than unity (i.e., $\delta(d_{\text{MAX}})^{\gamma(2)}$, $1/\beta(1)^{\gamma(2) - \gamma(1)}$). This is a first important outcome, which proves that densification does not always trigger an increase in the RFP, in contrast to the population's belief. On the other hand, the RFP at fixed distance is increased in S4, i.e., $\delta(P_{\text{TOT-FX}}^R) < 1$. Nevertheless, the RFP increase in this scenario depends solely on the sensitivity thresholds ratio $\delta(P_{\text{TH}}^R)$, and hence it can be easily controlled by the operator. In addition, we remind that S4 imposes both frequency and minimum sensitivity increases in deployment (2) w.r.t. deployment (1), while the level of densification is not varied. Eventually, the RFP at fixed distance in S5 includes terms that are greater than unity (i.e., $1/\beta(1)^{\gamma(2) - \gamma(1)}$ and $\delta(d_{\text{MAX}})^{\gamma(2)}$) and other ones that are instead lower than unity (i.e., $\delta(P_{\text{TH}}^R)$). Therefore, an approach based on numerical evaluation is required, in order to assess the impact on the RFP.

Focusing then on the expressions for the cell RFP ratio (right part of Tab. II), we can note that the terms $\delta(A)^{-1}$ and $\delta(d_{\text{MAX}}) = \frac{d_{\text{MAX}}(1)}{d_{\text{MAX}}(2)}$ appear in S1, S2, S3, and S5. Since $\delta(A)^{-1}$ is lower than unity while $\delta(d_{\text{MAX}})$ is greater than one, a numerical evaluation is required in order to assess the overall impact on the RFP ratio. On the other hand, $\delta(P_{\text{TOT-CELL}}^R) = \delta(P_{\text{TH}}^R)$ in S4, and consequently the same considerations already reported for $\delta(P_{\text{TOT-FX}}^R)$ hold also in this case.

In the following, we analyze the impact of the ELP setting on the RFP levels. We remind that ELP adjusts P^E in order to ensure the maximum PD limit at the border of the exclusion zone (i.e., at d_{MIN}), and therefore the radiated power does not scale with the maximum coverage distance d_{MAX} . Tab. III reports the closed-form expressions for $\delta(P_{\text{TOT-FX}}^R)$ and $\delta(P_{\text{TOT-CELL}}^R)$, by assuming $N^I = 0$. Interestingly, $\delta(P_{\text{TOT-FX}}^R)$ is equal to one in S1, meaning that the RFP at fixed distance is unchanged when passing from deployment (1) to deployment (2). On the other hand, the RFP tends to decrease in S3 and S4, since the term $\delta(f)^{-\eta}$ is clearly higher than unity. However, there are also cases in which the RFP ratio at fixed distance is increased in deployment (2) w.r.t. deployment (1). For example, $\delta(P_{\text{TOT-FX}}^R) < 1$ in S2, since the term $(\beta(1) \cdot d_{\text{MAX}})^{\gamma(2) - \gamma(1)}$ is lower than unity. In addition, a numerical evaluation of the formula is required in S5, since $(\beta(1) \cdot d_{\text{MAX}})^{\gamma(2) - \gamma(1)} < 1$ and $\delta(f)^{-\eta} > 1$. Focusing then on the cell RFP, $\delta(P_{\text{TOT-CELL}}^R)$ has to be numerically evaluated in S1, S2, S3, and S5 to assess the RFP increase/decrease. However, the cell RFP is surely decreased in S4, as the RFP ratio is equal to $\delta(f)^{-\eta}$, which is greater than one.

We then move our attention to the closed-form expressions of RFP when the contributions from neighbors are considered, i.e., $N^I > 0$. Intuitively, when introducing the P_{NEIGH}^R term of Eq. (12) in the RFP ratios, the closed-form expressions of $\delta(P_{\text{TOT-FX}}^R)$ and $\delta(P_{\text{TOT-CELL}}^R)$ become more complex than the $N^I = 0$ case reported in Tab. II-III. As a result, it is not possible to grasp the RFP increase/decrease by simply analyzing the terms appearing in the closed-form expressions. Therefore, rather than reporting such (complex) expressions, we directly compute $\delta(P_{\text{TOT-FX}}^R)$ and $\delta(P_{\text{TOT-CELL}}^R)$ from our models by applying the input parameters and then we analyze the outcomes in the following subsection.

TABLE III
CLOSED-FORM EXPRESSIONS FOR RFP RATIO AT FIXED DISTANCE $\delta(P_{\text{TOT-FX}}^R)$ AND CELL RFP RATIO $\delta(P_{\text{TOT-CELL}}^R)$ IN THE DIFFERENT SCENARIOS WHEN $N^I = 0$ (ELP CASE). TABLE BEST VIEWED IN COLORS.

Scenario	at Fixed Distance $\delta(P_{\text{TOT-FX}}^R)$		RFP Ratio	
	Formula	RFP Increase?	Cell $\delta(P_{\text{TOT-CELL}}^R)$	RFP Increase?
S1	1	No	$\delta(A)^{-1} \cdot \delta(d_{\text{MAX}})^{-1} \cdot \frac{d_{\text{MAX}}(1) - d_{\text{MIN}}}{d_{\text{MAX}}(2) - d_{\text{MIN}}}$	Num. Eval.
S2	$(\beta(1) \cdot d_{\text{MAX}}(1))^{\gamma(2) - \gamma(1)}$	Yes	$\delta(A)^{-1} \cdot \frac{\gamma(2) - 2}{\gamma(1) - 2} \cdot \left[\frac{d_{\text{MIN}}^{(2-\gamma(1))} - d_{\text{MAX}}(1)^{(2-\gamma(1))}}{d_{\text{MIN}}^{(2-\gamma(2))} - d_{\text{MAX}}(2)^{(2-\gamma(2))}} \right]$	Num. Eval.
S3	$\delta(f)^{-\eta}$	No	$\delta(A)^{-1} \cdot \delta(f)^{-\eta} \cdot \delta(d_{\text{MAX}})^{-1} \cdot \frac{d_{\text{MAX}}(1) - d_{\text{MIN}}}{d_{\text{MAX}}(2) - d_{\text{MIN}}}$	Num. Eval.
S4	$\delta(f)^{-\eta}$	No	$\delta(f)^{-\eta}$	No
S5	$(\beta(1) \cdot d_{\text{MAX}}(1))^{\gamma(2) - \gamma(1)} \cdot \delta(f)^{-\eta}$	Num. Eval.	$\delta(f)^{-\eta} \cdot \delta(A)^{-1} \cdot \frac{\gamma(2) - 2}{\gamma(1) - 2} \cdot \left[\frac{d_{\text{MIN}}^{(2-\gamma(1))} - d_{\text{MAX}}(1)^{(2-\gamma(1))}}{d_{\text{MIN}}^{(2-\gamma(2))} - d_{\text{MAX}}(2)^{(2-\gamma(2))}} \right]$	Num. Eval.

B. Numerical Evaluation of the RFP

We move our attention to the numerical evaluation of the RFP obtained by our models. This step is mandatory for the following reasons. First, it is possible to grasp the actual values of RFP increase/decrease, including the cases in Tab. II-III for which the RFP variation could not be preliminary determined. Second, we thoroughly evaluate the case with $N^I > 0$, i.e., the RFP includes the contributions from neighbors.

More formally, we adopt Eq. (9),(10),(12)-(16) to compute $\delta(P_{\text{TOT-FX}}^R)$ and $\delta(P_{\text{TOT-CELL}}^R)$ across the different scenarios, by selectively imposing $N^I = \{0, 6\}$ and P^E according to MSP or ELP setting. In order to better position the outcomes derived by our models, we also build a simple simulator coded in Matlab R2020a software that allows us to compute the RFP $P_{(p)}^R$ for each pixel p of the coverage area, by applying Eq. (1). To this aim, we assume a tessellation of non-overlapping squared pixels, each of them with 1×1 [m²] size. In addition, the pixel to gNB distance is computed from the center of the pixel. Focusing then on the computation of the RFP from neighboring gNBs done in the simulator, we assume the following cases: *i*) $N^I = 0$, in which $P_{(p)}^R$ is solely computed from the serving gNB, *ii*) $N^I = 6$, in which $P_{(p)}^R$ includes the RFP from the serving gNB and the RFP from the six closest neighboring gNBs w.r.t. the serving one. Given the RFP $P_{(p)}^R$ in each pixel, we then extract: *i*) the average RFP at fixed distance d_{FX} , computed over the pixels that are at distance $d_{(p,s)}$ within $d_{\text{FX}} - \epsilon \leq d_{(p,s)} \leq d_{\text{FX}} + \epsilon$, with $\epsilon = 1$ [m]; *ii*) the average cell RFP, computed over the pixels at distance $d_{\text{MIN}} \leq d_{(p,s)} \leq d_{\text{MAX}}$; *iii*) the RFP ratio at fixed distance and the cell RFP ratio, given the averages in *i*) and *ii*), computed over deployment (1) and deployment (2) for scenarios S1-S5.

Fig. 3 reports the numerical evaluation of the RFP ratios, by considering the MSP and ELP settings, the impact of neighbors, and the model vs. simulator outcomes. Before going into the details of each scenario, let us remind that the results obtained with our models for the $N^I > 0$ cases represent a worst-case, since the RFP from neighbors is conservatively evaluated with the UB of Eq. (12). We now analyze $\delta(P_{\text{TOT-FX}}^R)$ for the MSP case, shown in Fig. 3(a). Obviously, the RFP ratio at fixed distance is larger than unity for S1, S2, S3 (in accordance with Tab. II). Astonishingly, the RFP decrease is huge for all the scenarios introducing densification, since

$\delta(P_{\text{TOT-FX}}^R) \gg 1$. We remind that, in this case, we evaluate the RFP variation at distance d_{FX} from the serving gNB, i.e., close to d_{MIN} in our setting. Eventually, scenario S4 confirms the previously reported outcomes, i.e., a controlled RFP increase that depends on $\delta(P_{\text{TH}}^R)$. Finally, the numerical evaluation over S5 reveals a strong RFP reduction at fixed distance, i.e., up to around three orders of magnitude. Therefore, we can state that a strong densification dramatically reduces the RFP when this metric is evaluated in proximity to d_{MIN} .

We then move our attention to the RFP ratio at fixed distance for the ELP setting, visualized in Fig. 3(b). The results over scenarios S1, S3, S4 confirm the findings reported in Tab. III, with a huge RFP decrease in S3 and S4 (i.e., more than one order of magnitude in deployment (2) w.r.t. (1)). On the other hand, the RFP is increased in S2 (as expected). Finally, the numerical evaluation demonstrates that the RFP is reduced also in S5. By globally analyzing the outcomes of Fig. 3(b), we can state that densification with ELP setting does not increase the RFP at fixed distance in all scenarios except from S2.

In the following step, we evaluate $\delta(P_{\text{TOT-CELL}}^R)$, reported in Fig. 3(c) and in Fig. 3(d) for the MSP and ELP settings, respectively. Focusing on the MSP case (Fig. 3(c)), we can note that densification always reduces the average cell RFP, since $\delta(P_{\text{TOT-CELL}}^R) > 1$ in S1, S2, S3, S5. Again, this is an important outcome that contradicts the common belief of the population about exponential increase of RFP. In particular, the RFP decrease triggered by densification can be huge, i.e., around one order of magnitude in deployment (2) w.r.t. deployment (1) (scenarios S2 and S5). Clearly, $\delta(P_{\text{TOT-CELL}}^R) < 1$ in S4, in accordance with Tab. III. Focusing then on the ELP case (Fig. 3(d)), the cell RFP is decreased in S3 and S4. Not surprisingly, densification tends to increase the cell RFP in scenarios S1, S2 and S5. With the ELP setting, in fact, P^E does not scale with d_{MAX} , thus resulting in $\delta(P_{\text{TOT-CELL}}^R) > 1$ when densification is applied (except from scenario S3, which couples a light densification to a frequency increase).

Eventually, we compare the outcomes from our models (bars with label “model” in Fig. 3) w.r.t. the ones from the simulation (bars with label “simulation” in Fig. 3). Interestingly, our models for the RFP ratio nicely match the outcomes from simulations when $N^I = 0$. On the other hand, when $N^I > 0$, the RFP ratios predicted by the models are in general lower than the ones computed through simulation. This is however an

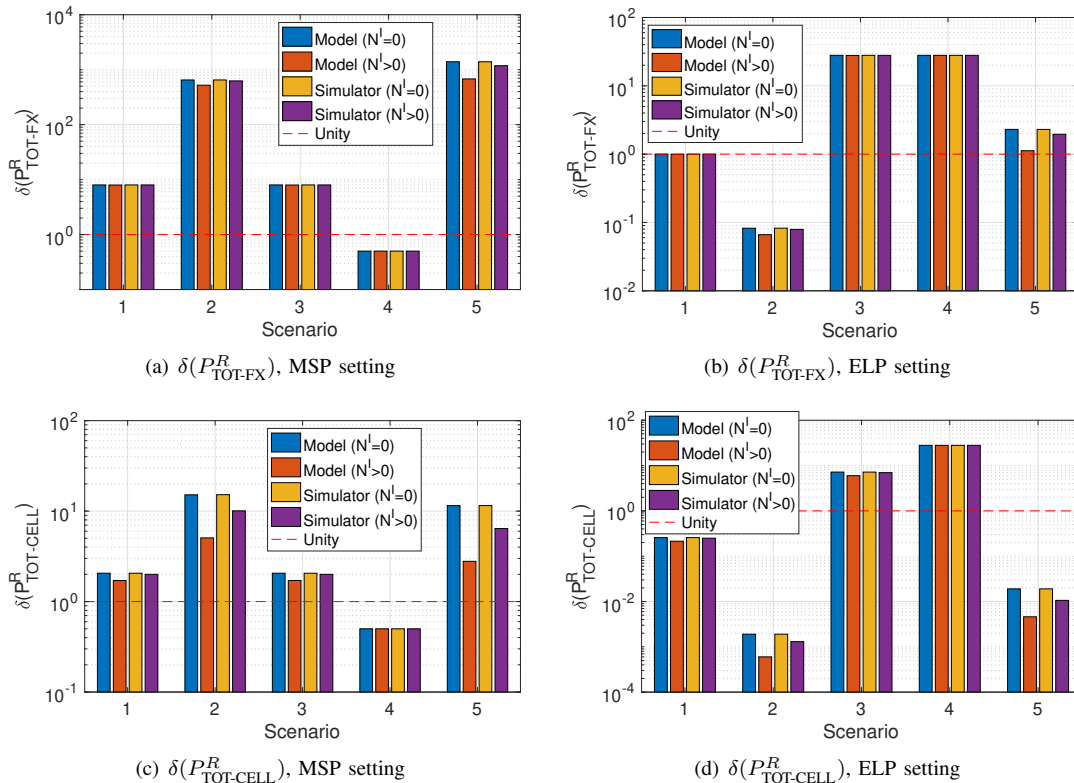


Fig. 3. Numerical evaluation of RFP by considering: RFP ratio at fixed distance $\delta(P_{\text{TOT-FX}}^R)$ vs. cell RFP ratio $\delta(P_{\text{TOT-CELL}}^R)$, ELP vs. MSP power setting, number of neighbors N^I equal to 0 or 6, model vs. simulation outcomes, and scenarios S1-S5. Figures best viewed in colors.

expected result, because the former adopts the UB at distance $(2\zeta - 1) \cdot d_{\text{MAX}}$, while the latter exactly computes the RFP for each distance $d_{(p,i)}$.

We then analyze in depth the differences between the RFP obtained from our models and the one computed from simulations. More in detail, we consider the variation of the fixed distance d_{FX} and its impact on the RFP model of Eq. (14). To this aim, we vary d_{FX} between d_{MIN} and d_{MAX} . Fig. 4 reports the RFP at fixed distance $P_{\text{TOT-FX}}^R$ in deployment (1) and in deployment (2) for scenario S5 with MSP setting (Fig. 4(a)) and S2 with ELP setting (Fig. 4(b)). The outcomes of our model are derived by imposing $N^I = 6$ neighboring gNBs. The figures report on the x-axis the distance percentage at which the RFP is evaluated, being 0% corresponding to $d_{\text{FX}} = d_{\text{MIN}}$ and 100% equal to the maximum one, i.e., $d_{\text{FX}} = d_{\text{MAX}}$. In addition to the outcomes from our models, we include the RFP from simulations, which is computed in this way: *i*) we generate a set of bins, each of them is size 1 [m], between d_{MIN} and d_{MAX} , *ii*) we compute the RFP for each pixel as per Eq. (1), *iii*) we assign each pixel to the bin that includes the pixel distance $d_{(p,s)}$, *iv*) we compute the average RFP for each bin, and finally *v*) we include in the plots of Fig. 4 only the bins having non-zero RFP values.

Several considerations hold by analyzing Fig. 4. First of all, the values of $P_{\text{TOT-FX}}^R$ obtained from our model are always higher than the ones computed from simulation. This result is expected, due to the UB from neighbors. In particular, the difference (in [dBm]) between the model and the simulation is proportional to the distance percentage, with lower RFP eval-

uation distances translating into smaller relative differences among model and simulation results and even overlapping RFP values. This is also an expected outcome, since we remind that, in proximity to the serving gNB, the RFP contributions from neighbors are in general negligible w.r.t. the RFP of the serving gNB. On the other hand, there are cases in which the RFP from neighbors is over-estimated by our model over the whole cell extent (e.g., deployment (2) in Fig. 4(a)). This is especially true for scenarios, like S5, in which the coverage size is extremely narrowed. In this way, we corroborate the findings of our models, which are derived under conservative and worst-case assumptions. Eventually, we can observe that $P_{\text{TOT-FX}}^R$ is a monotonic decreasing function w.r.t. the distance for both the model and the simulation (obviously). Finally, the comparison among deployment (1) and deployment (2) reveals that the RFP of the former is even lower than the latter for $\frac{d_{\text{FX}}}{d_{\text{MAX}}} \geq 0.4$ in S5 with MSP setting (Fig. 4(a)). On the other hand, for lower distances, the absolute RFP values are dramatically higher in deployment (1) w.r.t. (2). In addition, the slope of the RFP is notably increased as d_{FX} approaches d_{MIN} in deployment (1). Such details trigger another important consideration: densification is extremely effective in reducing the RFP for the users living in proximity to the installed gNBs and to achieve a uniform RFP distribution over the territory.

In the following step, we provide a visual representation of the pixel RFP $P_{(p)}^R$, computed by simulation from Eq. (1) in scenario S5 with $N^I = 6$ and MSP setting. Fig. 5 reports the obtained results over the two deployments. By comparing this

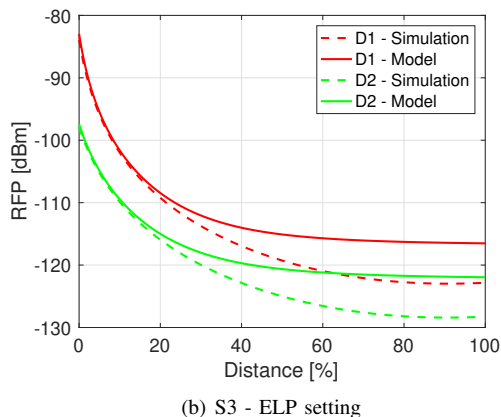
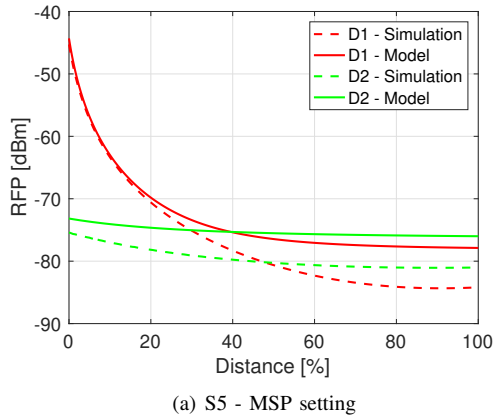


Fig. 4. RFP at fixed distance $P_{\text{TOT-FX}}^R$ in deployment (1) and deployment (2), computed with our model and by simulation. The figure reports $P_{\text{TOT-FX}}^R$ vs. the distance percentage for S5 with MSP setting (left) and for S3 with ELP (right).

figure against the popular belief of the population that was sketched in Fig. 1, several considerations can be drawn. First of all, the deployment of few gNBs does not necessarily mean low RFP over the territory, as the RFP tends to be pretty high in the zones that are close to the installed gNBs. For example, Fig. 5(a) shows that deployment (1) introduces huge RFP levels in proximity to the installed gNBs (i.e., the orange and the red zones in the figure), because the radiated power P^E is tuned to ensure the minimum sensitivity threshold $P_{\text{TH}}^R(1)$ at the cell edge $d_{\text{MAX}}(1)$. In addition, deploying a dense set of gNBs is not translated into an uncontrolled and exponential increase of RFP. In Fig. 5(b), in fact, the orange and red zones with large RFP completely disappear, since the coverage size of each cell is shrank in deployment (2) w.r.t. deployment (1), and hence P^E is now set to guarantee the minimum sensitivity at $d_{\text{MAX}}(2) < d_{\text{MAX}}(1)$. In addition, we remind that deployment (2) in this case also includes an increase of P_{TH}^R , and hence a better 5G service w.r.t. deployment (1). Despite this fact, however, the RFP appears more uniform in deployment (2) w.r.t. deployment (1).

C. Exclusion zone variation

When evaluating the RFP in scenario S5, a natural observation is that the exclusion zone for deployment (2) is pretty large compared to the coverage size. Although the rationale

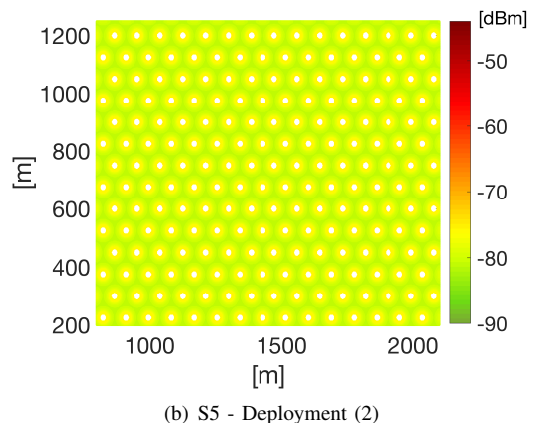
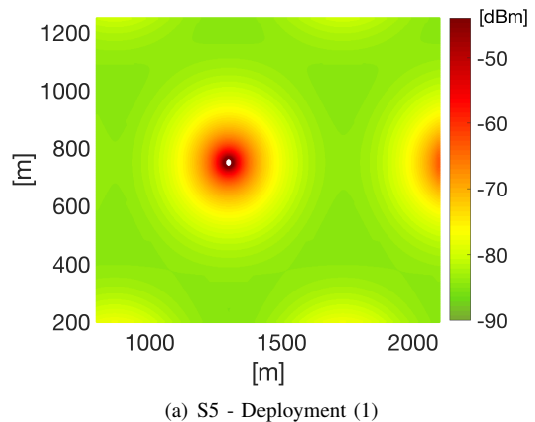


Fig. 5. RFP (in [dBm]) in scenario S5 for deployment 1 (left) and deployment 2 (right).

for choosing the size of the exclusion zone is clear (e.g., we adopt the same equipment type and a rooftop installation over the two candidate deployments), an interesting step would be to assess the impact on the RFP when the size of the exclusion zone in deployment (2) is reduced. More formally, let us denote the minimum distance with $d_{\text{MIN}}(1)$ and $d_{\text{MIN}}(2)$, respectively for deployment (1) and deployment (2). In addition, let us denote with $\delta(d_{\text{MIN}})$ the ratio among $d_{\text{MIN}}(1)$ and $d_{\text{MIN}}(2)$. Since $d_{\text{MIN}}(1) \neq d_{\text{MIN}}(2)$, we compare the two candidate deployments over two distinct fixed distances $d_{\text{FX}}(1)$ and $d_{\text{FX}}(2)$ (e.g., close to $d_{\text{MIN}}(1)$ for deployment (1) and close to $d_{\text{MIN}}(2)$ for deployment (2)).

Fig. 6 reports the numerical evaluation of MSP and ELP policies vs. different values of $d_{\text{MIN}}(2)$ (where $d_{\text{FX}}(2) = d_{\text{MIN}}(2) + 1$ [m]), while all the other parameters are kept unchanged w.r.t. the already presented ones. Interestingly, the decrease of $d_{\text{MIN}}(2)$ tends to reduce both $\delta(P_{\text{TOT-FX}}^R)$ and $\delta(P_{\text{TOT-CELL}}^R)$. This effect is expected for MSP, since the effective area covered by each cell in deployment (2) is increased as $d_{\text{MIN}}(2)$ is decreased. A similar trend is also observed in ELP. In particular, $\delta(P_{\text{TOT-FX}}^R)$ passes from values larger than unity when $d_{\text{MIN}}(2) = 15$ [m] to values lower than unity $d_{\text{MIN}}(2) = 5$ [m]. As a consequence, densification is not always beneficial in reducing the level of pollution at fixed distance in this case.

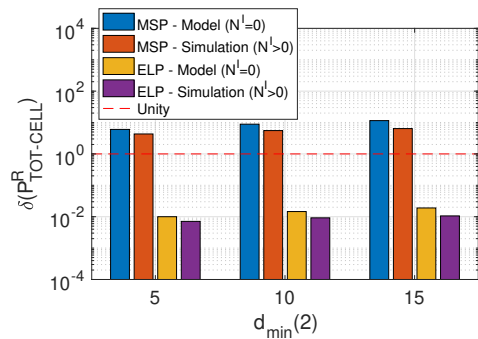
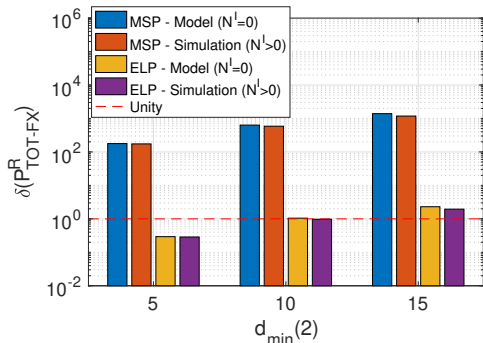
(a) $\delta(P_{\text{TOT-FX}}^R)$ (b) $\delta(P_{\text{TOT-CELL}}^R)$

Fig. 6. Impact of $d_{\text{MIN}}(2)$ variation on $\delta(P_{\text{TOT-FX}}^R)$ and $\delta(P_{\text{TOT-CELL}}^R)$ (S5 scenario).

D. Impact of spectrum-based power setting policies

A natural question is the following: Which is the impact of adopting other policies in setting the gNB radiated power? To answer such question, we have introduced a Spectrum-based Power Setting (SPS), based on the idea that the maximum radiated power is proportional to the amount of spectrum managed by the gNB. Actually, SPS-based policies are defined by different regulation authorities (e.g., Federal Communications Commission (FCC)) to set the maximum power radiated by the gNB, which is used during the planning of the network, e.g., when requesting permissions to install the gNB. For example, FCC defines a standardization 47 [dBm]/10 [MHz] for outdoor base stations that have to be installed at a height above 6 [m] from ground level [43]. However, we point out that the actual power radiated by the gNB in operation is typically order of magnitudes lower than the maximum one [26], thus resulting in a potential large over-estimation of RFP. Therefore, in the following, we evaluate the impact of SPS, by keeping in mind that the RFP may be largely over-estimated in this case. More formally, the power radiated by each gNB is then set to $P^E = P^F \cdot B/10$, where P^F is the maximum amount of radiated power over 10 [MHz] of bandwidth, and B is the adopted bandwidth (in MHz). We then express the RFP ratio at fixed distance $\delta(P_{\text{TOT-FX}}^R)$ and cell RFP ratio $\delta(P_{\text{TOT-CELL}}^R)$ by considering the SPS setting. Clearly, it holds that $P^E(1) = P^E(2)$ when $f(1) = f(2)$ (since $B(1) = B(2)$). Otherwise, when $f(1) \neq f(2)$, $B(1) \neq B(2)$ and consequently $P^E(1) \neq P^E(2)$.

We initially compute the closed form expressions of

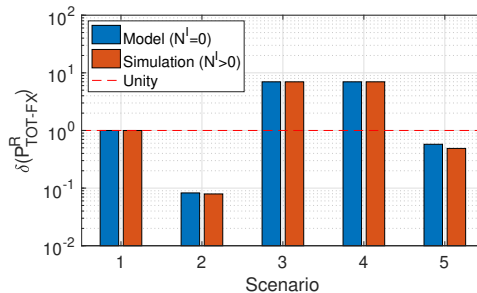
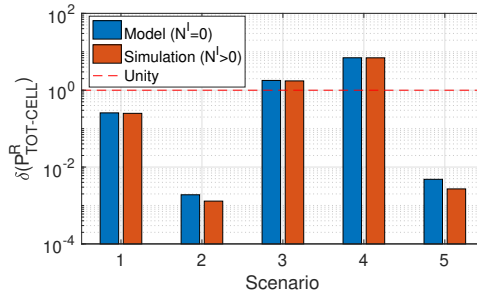
(a) $\delta(P_{\text{TOT-FX}}^R)$ (b) $\delta(P_{\text{TOT-CELL}}^R)$

Fig. 7. Impact of SPS policy on the RFP ratio at fixed distance $\delta(P_{\text{TOT-FX}}^R)$ and on average over the cell $\delta(P_{\text{TOT-CELL}}^R)$ over the different scenarios.

$\delta(P_{\text{TOT-FX}}^R)$ and $\delta(P_{\text{TOT-CELL}}^R)$ when $N^I = 0$ (not reported here due to the lack of space). In brief, the expressions of RFP are exactly the same of the ELP policy for S1 and S2 (since $P^E(1) = P^E(2)$). Therefore, for such scenarios, the same considerations already made for the ELP setting hold here. For S3-S5 (i.e., when f varies across the deployment), the closed-form expressions of RFP can be derived from the ELP ones by multiplying the terms of Tab. III for $\delta(B) = B(1)/B(2)$.

In the following step, numerically evaluate the SPS policy by imposing $B(1) = 20$ [MHz] when $f(1) = 700$ [MHz] and $B(2) = 3700$ [MHz] when $f(2) = 3700$ [MHz], in accordance with the 5G spectrum allocation currently enforced in Italy. Fig. 7 reports $\delta(P_{\text{TOT-FX}}^R)$ and $\delta(P_{\text{TOT-CELL}}^R)$ over the different scenarios. As expected, the RFP ratios of SPS are the same of ELP in both S1 and S2. Interestingly, a decrease of RFP in deployment (2) w.r.t. (1) is experienced in both S3 and S4 (at both fixed distance and on average over the entire cell). In particular, densification is able to reduce both $\delta(P_{\text{TOT-FX}}^R)$ and $\delta(P_{\text{TOT-CELL}}^R)$ in S3. Finally, an increase of RFP in deployment (2) is observed in scenario S5 (in line with ELP - when $\delta(P_{\text{TOT-CELL}}^R)$ is considered).

E. Impact of pollution from neighbors

In the last part of our work, we have shed light on the impact of pollution of neighbors, by including the contributions from the second level neighbors w.r.t. the serving gNB. Due to the lack of space, we summarize the main outcomes. In particular, we have computed the RFP from neighbors as the contributions from the six adjacent gNBs w.r.t. the serving one (i.e., the first level neighbors) plus the RFP generated by the gNBs that are adjacent to the six neighbors (i.e., the second level neighbors). Results, obtained from both model and simulation

across scenarios S1-S5 (MSP and ELP settings), reveal that the RFP is not highly affected by the second level neighbors. Therefore, we can conclude that the RFP is mainly impacted by the serving cell and the first level neighbors.

VI. SUMMARY AND FUTURE WORKS

We have analyzed the impact of cellular network densification on the RFP. Initially, we have proposed a simple model to compute the RFP from the serving gNB and a set of neighboring gNBs. In the following step, we have introduced the RFP ratios to compare the “pollution” variation among two distinct candidate 5G deployments. Results, obtained by solving the closed-form expressions for the RFP ratios in a set of meaningful 5G scenarios, prove that densification *does not* introduce an uncontrolled and exponential increase of RFP, thus dispelling this popular myth among the general public. On the contrary, we have demonstrated that densification strongly reduces the RFP (up to three orders of magnitude) when the radiated power is set according to MSP. On the other hand, when the radiated power is set in accordance with ELP, the RFP variation is always controlled. In this case, the RFP increase or decrease depends on the specific densification scenario under consideration. However, there are conditions under which the RFP is decreased by densification with ELP, e.g., when the frequency is increased in parallel to a light densification, without a change in the propagation exponents. Eventually, we have shown that the outcomes from the model are always in accordance w.r.t. the ones derived by simulation. Finally, we have analyzed the impact of different key parameters on the RFP (e.g., size of exclusion zone, alternative spectrum-based power policies to set the radiated power and increase of pollution from neighbors).

As future research activity, the adoption of detailed propagation models could be an interesting step, in order to consider the impact of shadowing/fading margins and changes in the propagation exponent across the extent of the cell. In addition, the evaluation of indoor 5G deployments adopting mm-Waves frequencies and femto cells is another attractive research direction. Eventually, we will consider the impact of non-regular deployments and/or coverage layouts on the RFP. Finally, the assessment of the RFP by adopting other exposure metrics, e.g., field strength and/or PD, is a promising future work.

ACKNOWLEDGEMENTS

We are grateful to Prof. Andrea Detti, the handling editor Prof. Kountouris and the anonymous reviewers for their fruitful suggestions on how to improve the work.

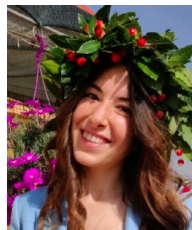
REFERENCES

- [1] L. Chiaraviglio, G. Bianchi, N. Blefari-Melazzi, and M. Fiore, “Will the Proliferation of 5G Base Stations Increase the Radio-Frequency ‘Pollution’?”, in *IEEE VTC2020-Spring*, pp. 1–7, IEEE, 2020.
- [2] *5G appeal: Scientists and doctors warn of potential serious health effects of 5G*. Available at <https://www.jrseco.com/wp-content/uploads/2017-09-13-Scientist-Appeal-5G-Moratorium.pdf>, last accessed on 25th Sept. 2020.
- [3] M. Simkó and M.-O. Mattsson, “5G wireless communication and health effects - a pragmatic review based on available studies regarding 6 to 100 GHz,” *Int. journal of environmental research and public health*, vol. 16, no. 18, p. 3406, 2019.
- [4] J. Bushberg, C. Chou, K. Foster, R. Kavet, D. Maxson, R. Tell, and M. Ziskin, “IEEE Committee on Man and Radiation - COMAR Technical Information Statement: Health and Safety Issues Concerning Exposure of the General Public to Electromagnetic Energy from 5G Wireless Communications Networks,” *Health Physics*, vol. 119, no. 2, p. 236, 2020.
- [5] *Red sky at night, cell tower’s alight: nearly half of UK consumers think 5G is a health risk*. Available at: <https://tinyurl.com/9crxx8uh>, Last Accessed: 25th Sept. 2020.
- [6] *The Deep Conspiracy Roots of Europe’s Strange Wave of Cell-Tower Fires*. Available at <https://www.politico.com/news/magazine/2020/05/18/deep-conspiracy-roots-europe-wave-cell-tower-fires-264997>, Last Accessed: 25th Sept. 2020.
- [7] *Papua New Guinea govt puts hold on 5G development*. Available at <https://www.rnz.co.nz/international/pacific-news/406411/png-govt-puts-hold-on-5g-development>, Last Accessed: 25th Sept. 2020.
- [8] *Jamaica must explore risks before adopting 5G tech, Robinson urges*. Available at http://www.jamaicaobserver.com/news/jamaica-must-explore-risks-before-adopting-5g-tech-robinson-urges_177268, Last Accessed: 25th Sept. 2020.
- [9] *Radiation concerns halt Brussels 5G development, for now*. Available at <https://www.brusselstimes.com/brussels/55052/radiation-concerns-halt-brussels-5g-for-now/>, Last Accessed: 25th Sept. 2020.
- [10] *Cities Are Saying No to 5G, Citing Health, Aesthetics - and FCC Bullying*. Available at: <https://tinyurl.com/e8td6t9f>, Last Accessed: 25th Sept. 2020.
- [11] *Before it’s too late*. Available at: <https://www.recorder.com/my-turn-frey-before-it-s-too-late-36084135>, Last Accessed: 25th Sept. 2020.
- [12] L. Chiaraviglio, A. Elzanaty, and M.-S. Alouini, “Health risks associated with 5g exposure: A view from the communications engineering perspective,” *arXiv preprint arXiv:2006.00944*, 2020.
- [13] L. Chiaraviglio, S. Rossetti, S. Saida, S. Bartoletti, and N. Blefari-Melazzi, ““pencil beamforming increases human exposure to electromagnetic fields”: True or false?,” *IEEE Access*, vol. 9, pp. 25158–25171, 2021.
- [14] M. Thurfjell, M. Ericsson, and P. de Bruin, “Network densification impact on system capacity,” in *2015 IEEE 81st vehicular technology conference (VTC Spring)*, pp. 1–5, IEEE, 2015.
- [15] V. M. Nguyen and M. Kountouris, “Performance limits of network densification,” *IEEE Journal on Selected Areas in Communications*, vol. 35, no. 6, pp. 1294–1308, 2017.
- [16] J. Liu, M. Sheng, L. Liu, and J. Li, “Network densification in 5G: From the short-range communications perspective,” *IEEE Communications Magazine*, vol. 55, no. 12, pp. 96–102, 2017.
- [17] X. Ge, S. Tu, G. Mao, C.-X. Wang, and T. Han, “5G ultra-dense cellular networks,” *IEEE Wireless Communications*, vol. 23, no. 1, pp. 72–79, 2016.
- [18] J. Park, S.-L. Kim, and J. Zander, “Asymptotic behavior of ultra-dense cellular networks and its economic impact,” in *2014 IEEE Global Communications Conference*, pp. 4941–4946, IEEE, 2014.
- [19] R. Arshad, H. ElSawy, S. Sorour, T. Y. Al-Naffouri, and M.-S. Alouini, “Handover management in 5G and beyond: A topology aware skipping approach,” *IEEE Access*, vol. 4, pp. 9073–9081, 2016.
- [20] J. G. Andrews, X. Zhang, G. D. Durgin, and A. K. Gupta, “Are we approaching the fundamental limits of wireless network densification?,” *IEEE Communications Magazine*, vol. 54, no. 10, pp. 184–190, 2016.
- [21] M. Shafi, A. F. Molisch, P. J. Smith, T. Haustein, P. Zhu, P. De Silva, F. Tufvesson, A. Benjebbour, and G. Wunder, “5G: A tutorial overview of standards, trials, challenges, deployment, and practice,” *IEEE journal on selected areas in communications*, vol. 35, no. 6, pp. 1201–1221, 2017.
- [22] S. Dang, O. Amin, B. Shihada, and M.-S. Alouini, “What should 6G be?,” *Nature Electronics*, vol. 3, no. 1, pp. 20–29, 2020.
- [23] E. J. Oughton, K. Katsaros, F. Entezami, D. Kaleshi, and J. Crowcroft, “An Open-Source Techno-Economic Assessment Framework for 5G Deployment,” *IEEE Access*, vol. 7, pp. 155930–155940, 2019.
- [24] L. Chiaraviglio, A. S. Cacciapuoti, G. Di Martino, M. Fiore, M. Montesano, D. Trucchi, and N. B. Melazzi, “Planning 5G networks under EMF constraints: State of the art and vision,” *IEEE Access*, vol. 6, pp. 51021–51037, 2018.

- [25] *D3.1–Study on Small Cells and Dense Cellular Networks Regulatory Issues*. Available at https://global5g.org/sites/default/files/Global5G.org-D3.1_Study%20on%20small%20cells%20and%20dense%20cellular%20networks%20regulatory%20issues_final.pdf, last accessed on 23rd September 2020.
- [26] D. Colombi, P. Joshi, B. Xu, F. Ghasemifard, V. Narasaraju, and C. Törnevik, “Analysis of the Actual Power and EMF Exposure from Base Stations in a Commercial 5G Network,” *Applied Sciences*, vol. 10, no. 15, p. 5280, 2020.
- [27] “C95.1-2019 IEEE standard for safety levels with respect to human exposure to radio frequency electromagnetic fields, 3 kHz to 300 GHz,” tech. rep., Institute of Electrical and Electronics Engineers (IEEE), New York, NY, US, 2019.
- [28] International Commission on Non-Ionizing Radiation Protection (ICNIRP), “ICNIRP guidelines on limiting exposure to time-varying electric, magnetic and electromagnetic fields (100 kHz to 300 GHz).” Available at: <https://www.icnirp.org/cms/upload/publications/ICNIRPrfgdl2020.pdf>, Jul. 2020. Last Accessed: 29th Sept. 2020.
- [29] *5G - Study on scenarios and requirements for next generation access technologies (3GPP TR 38.913 version 16.0.0 Release 16)*. Available at: https://www.etsi.org/deliver/etsi_tr/138900_138999/138913/16.00.00_60/tr_138913v160000p.pdf, Last Accessed: 23th March 2021.
- [30] T. S. Rappaport, Y. Xing, G. R. MacCartney, A. F. Molisch, E. Mellios, and J. Zhang, “Overview of millimeter wave communications for fifth-generation (5G) wireless networks with a focus on propagation models,” *IEEE Transactions on Antennas and Propagation*, vol. 65, no. 12, pp. 6213–6230, 2017.
- [31] B. Thors, A. Furuskär, D. Colombi, and C. Törnevik, “Time-Averaged Realistic Maximum Power Levels for the Assessment of Radio Frequency Exposure for 5G Radio Base Stations Using Massive MIMO,” *IEEE Access*, vol. 5, pp. 19711–19719, 2017.
- [32] D. Franci, S. Coltellacci, E. Grillo, S. Pavoncello, T. Aureli, R. Cintoli, and M. D. Migliore, “An experimental investigation on the impact of duplexing and beamforming techniques in field measurements of 5g signals,” *Electronics*, vol. 9, no. 2, p. 223, 2020.
- [33] S. Adda, T. Aureli, S. Coltellacci, S. D’Elia, D. Franci, E. Grillo, N. Pasquino, S. Pavoncello, R. Suman, and M. Vaccaroni, “A methodology to characterize power control systems for limiting exposure to electromagnetic fields generated by massive mimo antennas,” *IEEE Access*, vol. 8, pp. 171956–171967, 2020.
- [34] M. A. Jamshed, F. Heliot, and T. W. Brown, “A survey on electromagnetic risk assessment and evaluation mechanism for future wireless communication systems,” *IEEE Journal of Electromagnetics, RF and Microwaves in Medicine and Biology*, vol. 4, no. 1, pp. 24–36, 2019.
- [35] H. T. Friis, “A note on a simple transmission formula,” *Proceedings of the IRE*, vol. 34, no. 5, pp. 254–256, 1946.
- [36] *ITU-T K.52 : Guidance on complying with limits for human exposure to electromagnetic fields*. Available at <https://www.itu.int/rec/T-REC-K.52/en>, last accessed on 25th July 2018.
- [37] *IEC 62232:2017 Determination of RF field strength, power density and SAR in the vicinity of radiocommunication base stations for the purpose of evaluating human exposure*. Available at <https://webstore.iec.ch/publication/28673>, last accessed on 25th Sept. 2020.
- [38] *User Equipment (UE) radio transmission and reception; Part 1: Range 1 Standalone (3GPP TS 38.101-1 version 16.6.0 Release 16)*. Available at https://www.etsi.org/deliver/etsi_ts/138100_138199/13810101/16.06.00_60/ts_13810101v160600p.pdf, last accessed on 23th March 2021.
- [39] *ITU-T K Supplement 14 The impact of RF-EMF exposure limits stricter than the ICNIRP or IEEE guidelines on 4G and 5G mobile network deployment*. Available at https://www.itu.int/rec/dologin_pub.asp?lang=e&id=T-REC-K.Sup14-201909-1!!PDF-E&type=items, last accessed on 23th March 2021.
- [40] *ITU-T K.70 Mitigation techniques to limit human exposure to EMFs in the vicinity of radiocommunication stations*. Available at <https://www.itu.int/rec/T-REC-K.70-201801-I/en>, last accessed on 26th Feb. 2020.
- [41] L. Chiaraviglio, C. D. Paolo, G. Bianchi, and N. Blefari-Melazzi, “Is It Safe Living in the Vicinity of Cellular Towers? Analysis of Long-Term Human EMF Exposure at Population Scale,” in *2020 IEEE 91st Vehicular Technology Conference (VTC2020-Spring)*, pp. 1–7, 2020.
- [42] *5G - Study on channel model for frequencies from 0.5 to 100 GHz (3GPP TR 38.901 version 16.1.0 Release 16)*. Available at: https://www.etsi.org/deliver/etsi_tr/138900_138999/138901/16.01.00_60/tr_138901v160100p.pdf, Last Accessed: 23th March 2021.
- [43] *CFR 96.41 - General radio requirements*. Available at: <https://www.law.cornell.edu/cfr/text/47/96.41>, Last Accessed: 23th March 2021.



Luca Chiaraviglio (M’09-SM’16) is Associate Professor at the University of Rome Tor Vergata (Italy). He holds a Ph.D. in Telecommunication and Electronics Engineering, obtained from Politecnico di Torino (Italy). Luca has co-authored 150+ papers published in international journals, books and conferences. Luca has received the Best Paper Award at IEEE VTC-Spring 2020, IEEE VTC-Spring 2016 and ICIN 2018, all of them appearing as first author. Some of his papers are listed as Best Readings on Green Communications by IEEE. Moreover, he has been recognized as an author in the top 1% most highly cited papers in the ICT field worldwide. His current research topics cover 5G networks, optimization applied to telecommunication networks, electromagnetic fields and health risks assessment of 5G communications.



Sara Turco graduated in ICT and Internet Engineering from the University of Rome Tor Vergata in 2021. Between June 2020 and March 2021 she has been a CNIT Researcher. She currently works as Orizzonte Sistemi Navali S.p.A. as Integration Engineer.



Giuseppe Bianchi is currently a full professor at the Networking and Network Security, University of Roma Tor Vergata. His research interests include wireless networks (his pioneer work on WLAN modelling received the 2017 ACM SigMobile Test-of-Time Award), programmable network systems, security monitoring and vulnerability assessment, traffic modelling and control, and is documented in about 280 peer-reviewed international journal and conference papers, accounting for more than 20.000 citations (source: Google Scholar). He has coordinated six large scale EU projects, and has been (or still is) editor for several journals in his field, including the IEEE/ACM Transactions on Networking, the IEEE Transactions on Wireless Communications, the IEEE Transactions on Network and Service Management, and the Elsevier Computer Communications.



Nicola Blefari-Melazzi is currently a Full Professor of telecommunications with the University of Rome “Tor Vergata”, Italy. He is currently the Director of CNIT, a consortium of 37 Italian Universities. He has participated in over 30 international projects, and has been the principal investigator of several EU funded projects. He has been an Evaluator for many research proposals and a Reviewer for numerous EU projects. He is the author/coauthor of about 200 articles, in international journals and conference proceedings. His research interests include the performance evaluation, design and control of broadband integrated networks, wireless LANs, satellite networks, and of the Internet.